



A microfluidic chip using Au@SiO₂ array–based highly SERS-active substrates for ultrasensitive detection of dual cervical cancer–related biomarkers

Yingyan Gu^{1,2,3} · Zhiyue Li^{2,4} · Shengjie Ge^{1,3,5} · Yu Mao^{1,3,5} · Yuexing Gu^{1,3,5} · Xiaowei Cao^{1,3,5} · Dan Lu^{1,2,3,4}

Received: 19 July 2022 / Accepted: 17 August 2022 / Published online: 2 September 2022
© Springer-Verlag GmbH Germany, part of Springer Nature 2022

Abstract

In this work, a microfluidic chip using Au@SiO₂ array–based highly active SERS substrates was developed for quantitative detection of squamous cell carcinoma antigen (SCCA) and carcinoembryonic antigen (CEA) associated with cervical cancer. The chip consisted of six functional units with pump-free design, enabling parallel detection of multiple samples in an automatic manner without external pumps and improving the portability. Ag nanocubes (AgNCs) were labeled with Raman reporters and coupled with antibodies (labeling) to prepare SERS tags, while the Au nanoparticle–modified SiO₂ microsphere (Au@SiO₂) array was conjugated with antibodies (coating) to generate the highly SERS-active capturing substrate. In the presence of target biomarkers, they were captured by SERS tags and capturing substrate, resulting in the formation of “sandwich” structures which were trapped in the detection chamber. As the immune reaction proceeded, a large number of “hot spots” were generated by the proximity of the Au@SiO₂ array substrate and AgNCs, greatly amplifying SERS signals. With this chip, the limits of detection of the SCCA and CEA levels in human serum were estimated to be as low as 0.45 pg mL⁻¹ and 0.36 pg mL⁻¹, respectively. Furthermore, the good selectivity and reproducibility of this chip were confirmed. Finally, clinical serum samples were analyzed by this chip, and the outcomes were consistent with those of enzyme-linked immunosorbent assay (ELISA). Thus, the proposed microfluidic chip can be potentially applied for the clinical diagnosis of cervical cancer.

Keywords Microfluidic chip · Surface-enhanced Raman scattering · Ordered array · Cervical cancer · Biomarker

✉ Xiaowei Cao
cxw19861121@163.com

✉ Dan Lu
ludan1968@126.com

- ¹ Institute of Translational Medicine, Medical College, Yangzhou University, Yangzhou 225001, People's Republic of China
- ² Department of Obstetrics and Gynecology, College of Clinical Medicine, Yangzhou University, Yangzhou 225001, People's Republic of China
- ³ Jiangsu Key Laboratory of Integrated Traditional Chinese and Western Medicine for Prevention and Treatment of Senile Diseases, Yangzhou University, Yangzhou 225001, People's Republic of China
- ⁴ The First Clinical College, Dalian Medical University, Dalian 116011, People's Republic of China
- ⁵ Jiangsu Key Laboratory of Experimental & Translational Noncoding RNA Research, Medical College, Yangzhou University, Yangzhou 225001, People's Republic of China

Introduction

Cervical cancer is the fourth most prevalent malignancy found in women around the world [1]. What's more, it is estimated to affect 600,000 women worldwide each year, with more than 300,000 women dying as a result [2, 3]. Cervical cancer, like all cancers, has no obvious clinical symptoms and is difficult to detect in its early stage. Early detection of cervical cancer leads to successful treatment and favorable outcomes, whereas patients in advanced stages have terrible prognoses, with a 5-year survival rate of only 17% [4]. Therefore, looking for relevant biomarkers is urgent to assist the diagnosis of early-stage cervical cancer. Squamous cell carcinoma antigen (SCCA) is a well-known biomarker which is the most common and reliable biomarker for squamous cell carcinomas [5]. Given that squamous cell sarcoma accounts for ~70–80% of cervical cancers, SCCA can be considered one of the target biomarkers for cervical cancer detection [6]. Carcinoembryonic antigen (CEA) is

a broad-spectrum biomarker that indicates the existence of various cancers and tumors in the body [7]. As reported, CEA expression increases in cervical cancer patients, so it is commonly used for the detection of cervical cancer [8, 9]. Traditional methods for measuring biomarkers include enzyme-linked immunosorbent assay (ELISA), western blot, and mass spectrometry [10–12]. However, these techniques are complex and time-consuming and require experienced personnel to perform. Hence, it is demanding to develop handy techniques for quantitatively detecting SCCA and CEA in clinical samples.

In past decades, surface-enhanced Raman scattering (SERS)-based microfluidic chips have made tremendous progress in the field of biosensing [13–15], providing a new approach for the detection of various disease-related biomarkers. The combination of SERS and microfluidic system has both the advantages of them such as fingerprint characteristic, high sensitivity, low reagent consumption, and high throughput [16–18]. These benefits have substantially facilitated quantitative SERS analysis and have attracted growing interest from a variety of research groups. Recently, Mishra et al. [19] implemented an automated detection platform for multiple prostate cancer tumor markers using microfluidic chips. Ahi et al. [20] developed a capillary-driven microfluidic chip-based immunoassay using SERS as detection and successfully used it for the detection of hCG in urine samples. Gao et al. [21] reported a pump-free microfluidic chip for detection of the PSA level without manual incubation and a heavy syringe pump. These studies demonstrated that pump-free microfluidic chips could drive autonomous liquid flow via capillary pressure, making them more portable and easier to handle than traditional SERS microfluidic chips which require external pumps. At present, there are two ways to generate sufficient capillary pressure to allow a spontaneous flow of the liquid in the microfluidic chip, including increasing the internal surface area and applying a hydrophilic coating to the microchannel wall [22]. The comb-like structure at the end of each unit can increase the internal surface area and polyethylene glycol (PEG) treatment can improve the hydrophilic properties of the microchannel. Herein, the application of the two methods can give the microfluidic chip sufficient capillary pressure to drive automatic flow.

Since pump-free design can make SERS microfluidic chip detection easy to operate, SERS substrates are the key to SERS detection [23]. Thus, the study of SERS-active substrates in microfluidics has become an important research topic in recent years to realize SERS microfluidic chips with high sensitivity, good reproducibility, and high integration [24, 25]. Colloid-based nanoparticle substrates in microfluidics have some limitations, including low mixing efficiency, potential sample contamination, and low reproducibility [23]. Fortunately, these drawbacks can be overcome

by arranging disordered nanoparticles into a single layer of ordered nanoarrays. The highly ordered SERS-active substrates can provide outstanding signal uniformity and reproducibility due to their ordered structure [26–28]. As is common knowledge, the signal amplification of SERS is due to “hot spots” which are the electromagnetic fields excited by the localized surface plasmon resonance (LSPR) of nanomaterials [29–31]. The “hot spots” generally generated in the gap between two closely spaced nanoparticles [32]. The Au nanoparticle-modified SiO₂ microspheres (Au@SiO₂) array is ordered with uniform nanogaps. There are numerous gaps between adjacent gold nanoparticles which covered on the perfectly aligned SiO₂, creating high-density “hot spots.” And Au@SiO₂ array possesses increased surface area to adsorb more antibodies. In addition, among numerous techniques which can produce ordered nanoarrays, self-assembly method is simple, fast, and economical [33]. Other techniques such as nanolithography and template-assisted fabrication require expensive facilities and rigorous processes [34, 35].

In this work, we introduced a SERS microfluidic chip by employing Au@SiO₂ array-based highly SERS-active substrate for simultaneous detection of SCCA and CEA in clinical serum. Here, 4-mercaptobenzoic acid (4-MBA) and 5,5'-dithiobis-(2-nitrobenzoic acid) (DTNB) were selected as Raman reporters, which were labeled on the AgNCs and coupled with antibodies (labeling) to prepare two SERS tags. Meanwhile, Au@SiO₂ arrays were manufactured by the self-assembly method, and antibodies (coating) were immobilized on Au@SiO₂ arrays to create capturing substrates. Then, capturing substrates were integrated into the detection chamber of the SERS microfluidic chip. With samples and SERS tags added to the chip, SCCA and CEA were captured by the corresponding antibodies on SERS tags and capturing substrate, forming “sandwich” immunocomplexes for quantitative detection of dual cervical cancer-related biomarkers. Next, the selectivity, producibility, and sensitivity of this chip were assessed. Finally, the clinical samples were tested by using this chip and ELISA, and the obtained results were compared to confirm the feasibility of the chip.

Experimental section

Materials

Hexadecyl trimethyl ammonium bromide (CTAB), chlorauric acid (HAuCl₄), sodium borohydride (NaBH₄), silver nitrate (AgNO₃), silver trifluoroacetate (CF₃COOAg), ascorbic acid (AA), phosphate-buffered saline (PBS) (10 mM Na₂HPO₄, 10 mM NaH₂PO₄, pH 7.4), ethylene glycol (EG), polyethylene glycol (PEG), potassium carbonate (K₂CO₃), and hydrogen peroxide (H₂O₂) were all purchased from

Sinopharm Chemical Reagent Co. Ltd (China). 4-mercaptobenzoic acid (4-MBA), 5,5'-dithiobis-2-nitrobenzoic acid (DTNB), ammonium hydroxide (NH₄OH), methanol, and bovine albumin (BSA) were purchased from Sigma-Aldrich. Sodium hydroxide (NaOH), dimercaptosuccinic acid (DMSA), ethyl orthosilicate (C₈H₂₀O₄Si), and sodium dodecyl sulfate (SDS) were purchased from Noah Chemical Co. Ltd. (Yangzhou, China). Trisodium citrate dihydrate (Na₃C₆H₅Na₃O₇·2H₂O), N-hexane (C₆H₁₄), chloroform (CHCl₃), and glasses were all provided by Younuo Chemicals Co. Ltd (Yangzhou, China). All reagents can be used directly without further purification. ELISA kits, AFP, OPN, SCCA monoclonal antibody (labeling), CEA monoclonal antibody (labeling), SCCA polyclonal antibody (coating), and CEA polyclonal antibody (coating) were provided by Sangong Biotechnology Company (Shanghai, China). In all experiments, water was used directly from Milli-Q (resistivity > 18 M Ω cm, Millipore, USA) without any modification.

Serum sample collection and processing

The serum samples were provided by 90 female donors, all of whom were from the College of Clinical Medicine of Yangzhou University. The serum samples were divided into three groups: the healthy group, the cervical intraepithelial neoplasia (CIN) group, and the cervical cancer group, as indicated in Table 1. The healthy group was in generally good physical condition, and no malignant tumors were discovered during physical examination. The CIN and cervical cancer groups had all been diagnosed with clear imaging and pathology diagnosis, and none had received therapy prior to enrollment. Each sample provider gave 5 mL of venous blood in the morning before breakfast. The serum samples were achieved by centrifugation at 3000 rpm (5 °C) after 10 min and stored at -80 °C for testing.

Synthesis of AgNCs

The preparation procedures of AgNCs were according to Xia's methodology with a slight modification [36]. In the synthesis, Ag seeds were firstly prepared using the polyol process, with EG as the solvent and CF₃COOAg as the precursor to elemental silver. Then, AgNCs were obtained by the seed-mediated method. Briefly, 20 mL EG was

placed into a 100-mL vial. The EG solution was stirred and heated in an oil bath at 150 °C for 10 min. Six milliliters of poly(vinyl pyrrolidone) (PVP; 20 mg mL⁻¹, in EG) was added. After another 10 min, 50 mL of the as-prepared Ag seeds (1.1 × 10¹² particles mL⁻¹) in EG solution was introduced, followed by the addition of 200 mL AgNO₃ (282 mM, in EG). The growth was terminated after 3 h by quenching the reaction with an ice-water bath. All the products were centrifuged, followed by washing with acetone and deionized water to remove excess reactants. The final product was dispersed in deionized water for further use.

Preparation of Au@SiO₂ array substrate

Synthesis of SiO₂ microspheres

The modified Stöber method was used to create SiO₂ microspheres [37]. In brief, 10 mL of ethyl orthosilicate was added dropwise to a 30 °C-heated mixture of 10 mL ammonium hydroxide, 50 mL ethanol, and 6 mL ultrapure water. The fluid gradually changed color to a milky white. SiO₂ microspheres were obtained after 12 h of reaction. SiO₂ microspheres suspension was produced by centrifugation (4000 rpm, 15 min) to eliminate unreacted chemicals. Finally, SiO₂ microspheres were disseminated in methanol solution with a concentration of 5 wt%.

Synthesis of AuNPs

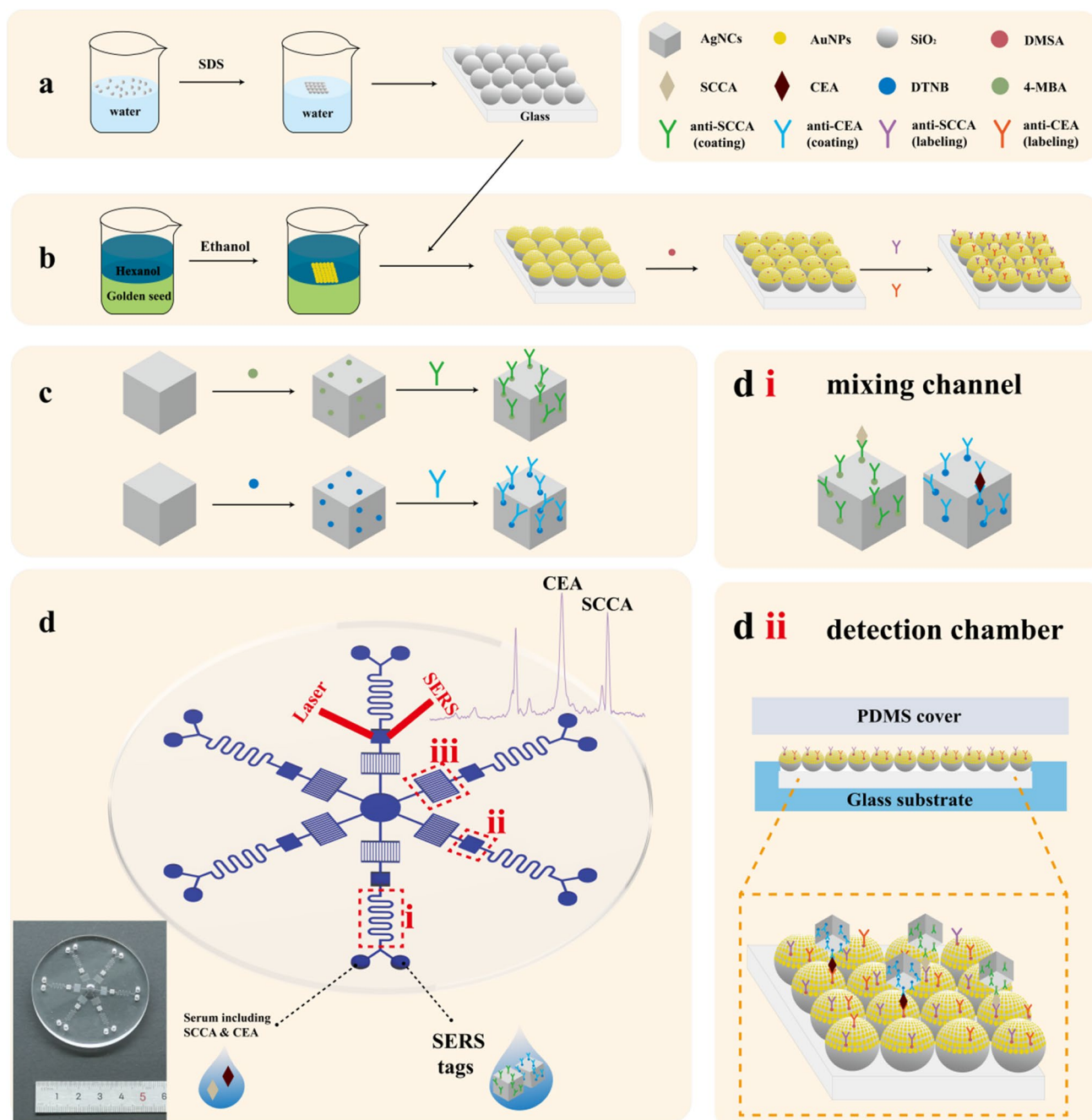
Au nanoparticles (AuNPs) were synthesized using the citrate-reduction process. Typically, 25 mL of HAuCl₄ (1 mM) was added into a 200-mL beaker and heated to boil. Then, under vigorous stirring, 4 mL of trisodium citrate solution (38 mM) was added. The solution was boiled for 15 min, during which it changed color from light yellow to vivid red. AuNP solution was obtained after cooling to room temperature.

Preparation of SiO₂ array

The Langmuir-Blodgett (L-B) gas-liquid interface assembly method was used to assemble the SiO₂ array [38]. The chloroform was mixed with SiO₂ microspheres suspension in a 2:3 volume ratio, and afterwards, 5 mL of the mixture was dropped on the water surface at a time. SiO₂ microspheres spontaneously diffused across the water surface until they covered the entire surface. Then, 100 mL SDS (2 wt%) solution was dropped on the water surface, causing a densely arranged SiO₂ array to be formed, which was then transferred to a clean hydrophilic glass. The glass with SiO₂ array was dried for further use.

Table 1 Basic characteristics of the included subjects

Group	Healthy people	CIN	Cervical cancer
Age (mean)	40	47	51
Specimen	30	30	30



Scheme 1 **a** Preparation of SiO₂ array. **b** Preparation of Au@SiO₂ array substrate and capturing substrate. **c** Fabrication of SERS tags. **d** Schematic illustration of the pump-free microfluidic chip for SERS

detection of SCCA and CEA. The chip contained three functional sections: (i) mixing channel, (ii) detection chamber, (iii) capillary pump

Preparation of Au@SiO₂ array substrate

The procedure of preparing the Au@SiO₂ array substrate is shown in Scheme 1a and b. Firstly, the oil–water interface self-assembly approach was used to create the AuNP array [39]. In the beaker, 4 mL of prepared AuNP solution and 2 mL of hexane were added sequentially followed by

2 mL of ethanol added drop by drop. During the ethanol addition process, a layer of metallic luster film, which was an AuNP array, was gradually produced. Next, the glass with assembled SiO₂ array was used to pick up the AuNP array. Thus, the Au@SiO₂ array substrate was prepared after drying.

Fabrication of SERS tags

In the process of fabricating SERS tags (AgNCs^{4-MBA}@anti-SCCA and AgNCs^{DTNB}@anti-CEA), 4-MBA and DTNB were used as Raman reporters, EDC and NHS served as coupling agents. 100 μ L of 4-MBA (10 mM, in ethanol) was added to 5 mL of the as-prepared AgNC solution and stirred for 2 h at room temperature. Next, the mixture was centrifuged at 8000 rpm for 15 min to remove the excess 4-MBA, the supernatant was discarded, and the precipitates were re-dispersed into 5 mL deionized water. This procedure was repeated twice. Subsequently, the sedimented 4-MBA labeled AgNCs (AgNCs^{4-MBA}) were suspended in 5 mL of PBS using ultrasonic oscillation. Later, 50 μ L EDC (150 mM) and 50 μ L NHS (30 mM) were dropped into the above solution in sequence. After shaking for 1.5 h, AgNCs^{4-MBA} with activated carboxylate terminals were achieved and ready to combine with antibodies (labeling). Then, 10 μ L anti-SCCA (labeling) (1 mg mL⁻¹) were added, incubating at 37 °C for 2 h. Finally, 1 mL of 5% BSA was added to the mixture and reacted for 3 h to block the unspecific binding sites on the surface of the particles. AgNCs^{4-MBA}@anti-SCCA were finally obtained via centrifugation (7000 rpm for 20 min) to remove excess antibodies, washed twice with PBS, and stored at 4 °C until use. The other SERS tags (AgNCs^{DTNB}@anti-CEA) were fabricated according to the same procedures.

Fabrication of capturing substrate

The anti-SCCA (coating) and anti-CEA (coating) were conjugated with Au@SiO₂ array substrate to create capturing substrate. Briefly, the prepared Au@SiO₂ array substrate was soaked in 2 mM DMSA solution for 3 h and then washed with PBS to remove free DMSA. Following that, the carboxy groups on the DMSA surface were activated by immersing them in the solution containing freshly prepared EDC (150 mM) and NHS (30 mM). One hour later, PBS was used to clean the substrate. Then, anti-SCCA (coating) and anti-CEA (coating) (10, μ L 1 mg mL⁻¹) were conjugated on the surface of the carboxy groups on the DMSA and incubated at 37 °C for 2 h. The extra antibodies were eliminated by PBS. Eventually, 5% BSA was used to fill the unmodified gaps left by DMSA or antibodies. After being cleaned with PBS, capturing substrate was fabricated.

Chip design and production

A pump-free microfluidic chip was created with capturing substrate integrated into the detection chamber for SERS immunoassay. The actual appearance of the chip is shown in Scheme 1c. The schematic diagram of microfluidic chip synthesis is shown in Fig. S1, the chip contained two parts:

PDMS cover and glass substrate. There were six functional units symmetrically distributed on the chip, each consisting of inlets, mixing channel, detection chamber built with capturing substrate, and comb-like structure acting as a capillary pump. The microchannels were 80 μ m in height and 200 μ m in width. The design drawing was first created by a CAD program. After that, a UV photoresist was used to produce the PDMS cover mold. Next, PDMS prepolymer and curing agent were mixed in a 10:1 ratio, then poured onto the mold. After being cured in an oven at 80 °C, the PDMS replica was separated from the mold. The glass substrate had six recesses by laser etching. Next, to increase capillary pressure, the microchannel walls underwent hydrophilic surface treatment with PEG. In the process, the as-prepared PDMS replica and glass substrate were ultrasonically cleaned with isopropanol and acetone solutions for 5 min, then rinsed with deionized water. After drying, the PDMS replica was exposed to oxygen plasma for 90 s and immediately coated by PEG, then moved to a hot plate at 150 °C for heating. Afterwards, it was cleaned with isopropanol and deionized water to eradicate excess PEG. The PDMS cover and glass substrate were laminated after placing capturing substrates into the recesses on the glass substrate (Fig. S1b). Finally, a SERS microfluidic chip ready for experiments was completely fabricated.

SERS measurement

First, a 10 μ L sample solution was added to one inlet, and the mixed solution of SCCA SERS tags (5 μ L) and CEA SERS tags (5 μ L) was added to the other inlet, as displayed in Scheme 1. After reaction about 30 min, a Renishaw inVia micro-Raman microscope fitted with a 50 \times objective and a 785 nm laser was employed for SERS measurements. The chosen laser power and integration time were 5 mW and 10 s, respectively. The laser was focused on the detection chamber and scanned at five random locations with a 20 mm² spot size in the range of 600–1800 cm⁻¹ to get the average SERS spectrum. All the tests were conducted at room temperature.

Characterization

To characterize the morphology of nanomaterials, the SEM images were acquired by the S-4800 II field-emission scanning electron microscope (Hitachi, Japan). High-resolution TEM (HRTEM) images and selected-area electron diffraction (SAED) were obtained using an emission transmission electron microscope (FEI, USA). A UV-vis spectrometer (AOE, China) was used to measure the absorption spectra of ultraviolet-visible-near infrared (UV-vis-NIR). Fourier transform infrared spectroscopy (FT-IR) analyses were

carried out on a Cary 610/670 Microscopic infrared spectrometer (Varian, USA).

Result and discussion

The workflow of the SERS-based pump-free microfluidic chip

A SERS-based pump-free microfluidic chip with highly SERS-active capturing substrates was developed for the immunoassay process and SERS detection in this work, the workflow of which is described in Scheme 1. Au@SiO₂ arrays were successfully prepared, and antibodies (coating) were attached with Au@SiO₂ arrays to synthesize capturing substrates (Scheme 1a and b). The capturing substrates were immobilized in the detection chambers of the chip, the fabrication process of which is presented in Fig. S1b and S1c. 4-MBA and DTNB were chosen to prepare two SERS tags due to their distinguished Raman peaks, which were modified on the AgNCs and bound with antibodies (labeling) (Scheme 1c). The working principle of the serum sample detection process was as follows: the serum and the SERS tags solution were added to the chip through two inlets. When liquids met up with the channel surface, they were automatically propelled along the mixing channels for further mixing and reaction. In the process,

if the target biomarkers (SCCA and CEA) were existent, they interacted and conjugated with anti-SCCA (labeling) or anti-CEA (labeling) on SERS tags, respectively. Later, the conjugations reached a detection chamber, which contained capturing substrate. The conjugations were captured by the antibodies (coating) immobilized on capturing substrate, establishing “sandwich” structures. At the same time, a massive number of “hot spots” were generated due to the proximity of Au@SiO₂ array substrate and AgNCs, considerably magnifying SERS signals. Finally, the laser was directed to the detection chamber for SERS measurement of the “sandwich” structures trapped within it. The intensity of SERS signals was correlated with the target concentration. According to the linear relationships between the logarithm of the SCCA concentration and the SERS intensity of 4-MBA at 1594 cm⁻¹ as well as between the logarithm of the CEA concentration and the SERS intensity of DTNB at 1330 cm⁻¹, the expression levels of SCCA and CEA could be determined indirectly.

Characterization of AgNCs

As illustrated in Fig. 1, the structure of the AgNCs was characterized. Transmission electron microscope (TEM) and scanning electron microscope (SEM) pictures of AgNCs (Fig. 1a and b) indicated that AgNCs with sharp corners and edges were successfully fabricated. Each edge of AgNCs

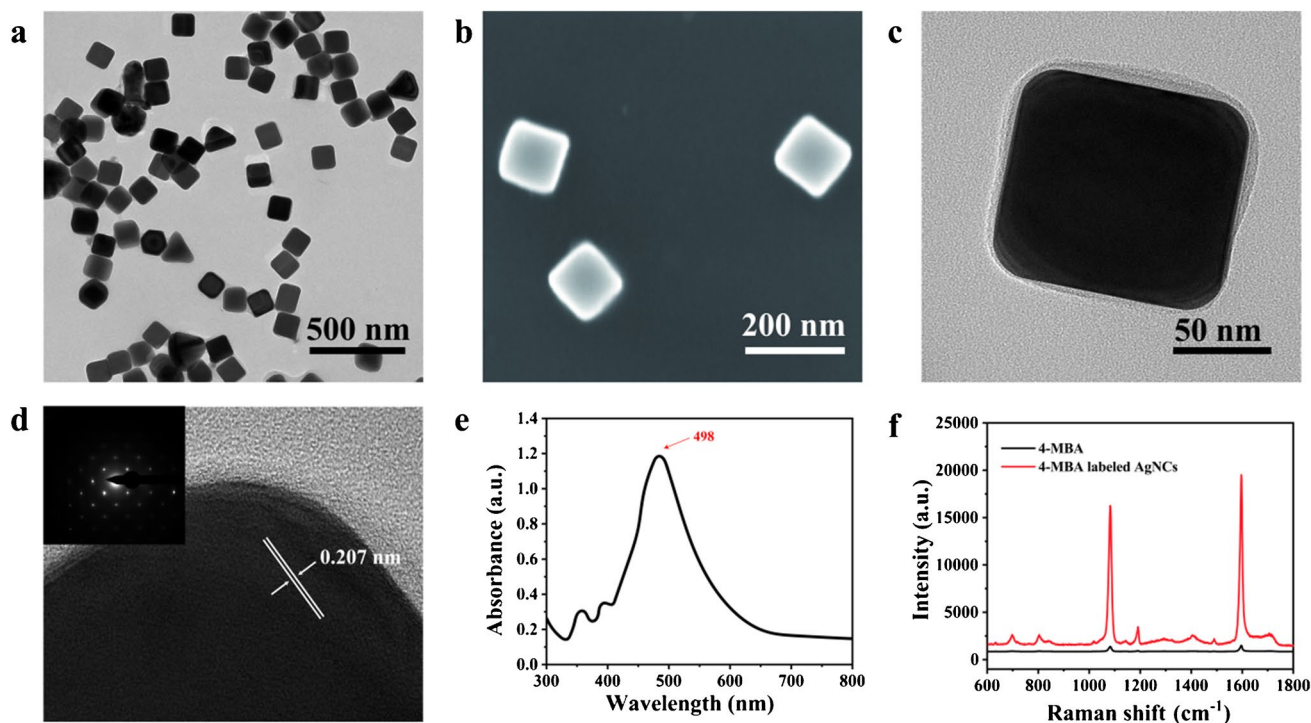


Fig. 1 a TEM image, b SEM image, c HRTEM image, d SAED pattern, and e UV–visible spectrum of AgNCs. f Raman spectra of 4-MBA labeled AgNCs and pure 4-MBA

was about 100 nm. Figure S2 shows the size distribution histogram of AgNCs, indicating the prepared AgNCs had about 95–105-nm edge length with uniform size distribution. The HRTEM image (Fig. 1c) and a partial magnification of the HRTEM image (Fig. 1d) depicted a lattice fringe spacing of 0.207 nm in AgNC. The insert of Fig. 1d demonstrated an electron diffraction pattern received by placing an electron beam perpendicular to a single nanocube, verifying that AgNCs were single crystals. As a noble metal nanomaterial, AgNCs had excellent optical properties and good surface plasmon resonance properties. Its main surface plasmon resonance peak (SPR) at 498 nm was caused by dipole plasmon resonance, and the relatively weak shoulder peaks appearing to the left of the main peak were caused by quadrupole plasmon resonance (Fig. 1e). Figure 1f illustrates the SERS enhancement effect of AgNCs. The Raman spectrum

of pure 4-MBA (10^{-2} M) was too faint to be easily seen in the absence of plasmonic metallic particles. However, the prominent characteristic peaks of the 4-MBA at 1083 cm^{-1} and 1594 cm^{-1} were clearly identified and considerably enhanced in the SERS spectrum of 4-MBA (10^{-6} M) labeled AgNCs, which was attributed to the formation of “hot spots” at the corners of individual AgNC and the increased electromagnetic fields between neighboring AgNCs. Thereby, AgNCs might be promising to prepare SERS probes.

Characterization of Au@SiO₂ array substrate

Scheme 1a and b clearly show the manufacturing process of the Au@SiO₂ array substrate. Figure 2a depicts the fabrication process of the AuNP array in detail. The inserted photo obviously showed a layer of Au film at the oil–water

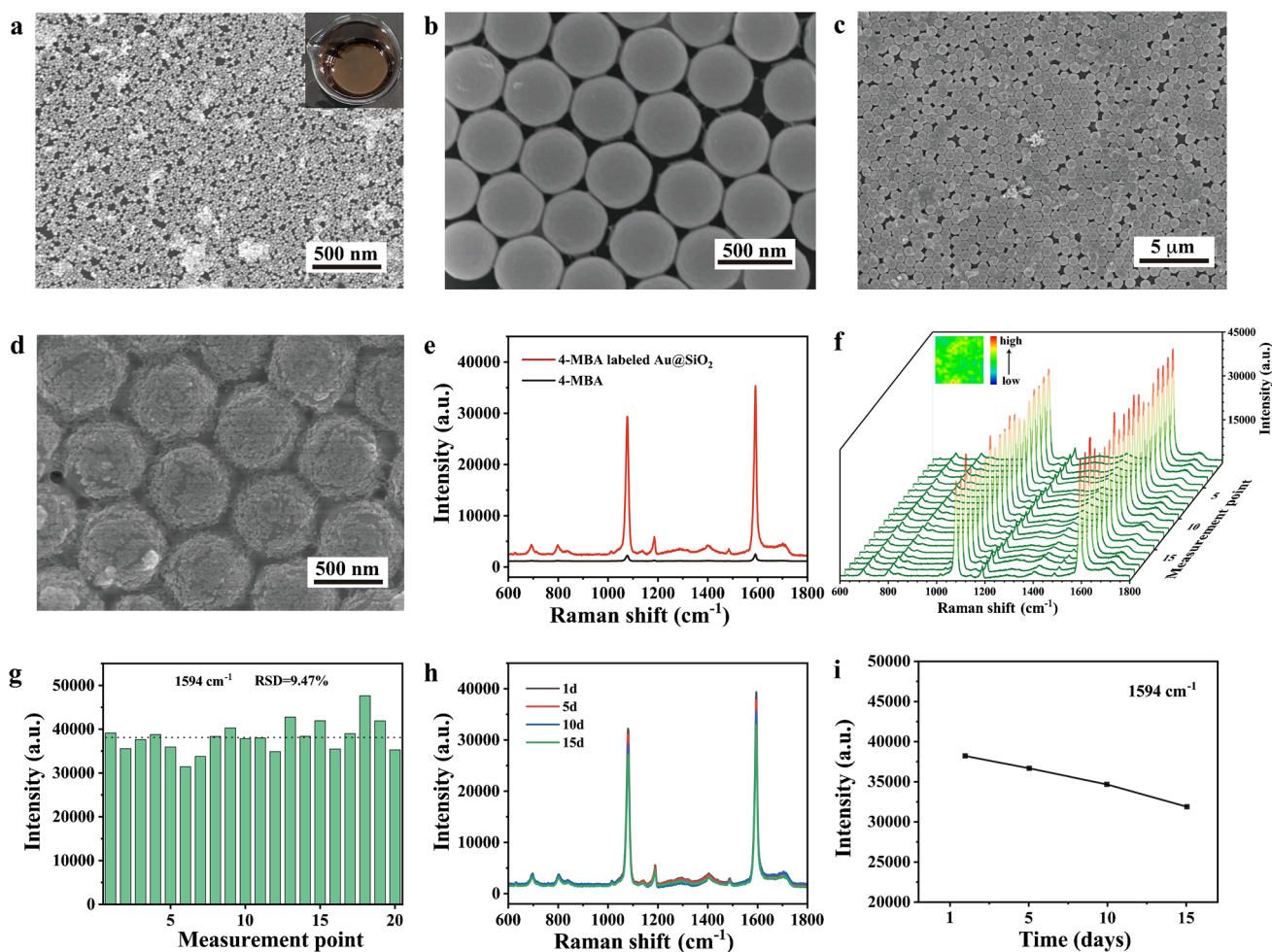


Fig. 2 SEM images of **a** AuNP arrays obtained by self-assembly of the oil–water interface, **b** SiO₂ array prepared by L-B method. **c** Low-magnification and **d** high-magnification SEM images of Au@SiO₂ array substrate. **e** Raman spectra of 4-MBA labeled Au@SiO₂ array substrate and pure 4-MBA. **f** SERS mapping of 4-MBA labeled Au@SiO₂ array substrate and SERS spectra of twenty points ran-

domly selected on Au@SiO₂ array substrate. **g** Intensity bar graphs of characteristic peak at 1594 cm^{-1} for the twenty points. **h** The average SERS spectra of 4-MBA labeled Au@SiO₂ array substrate after being stored for 1, 5, 10, 15, days. **i** The corresponding line chart of the signal intensities at 1594 cm^{-1}

interface, which was formed due to the different densities between hexane and AuNP solution. After the addition of ethanol, the charge density on the surface of AuNPs was reduced, allowing the gold nanoparticles to self-assemble and form an AuNP array at the oil–water interface. The SEM graph demonstrated that AuNPs were neatly ordered and uniformly dispersed at the oil–water interface with a diameter of approximately 20 nm. Structures of SiO₂ in spherical shape are clearly observed in Fig. 2b. SiO₂ microspheres had smooth surfaces with a size of about 450 nm. SiO₂ arrays were prepared by the L-B method. In such a method, SDS, as a surfactant, was absorbed on the surface of SiO₂ microspheres, resulting in the development of clusters of SiO₂ microspheres. Simultaneously, it increased hydrophobic contacts between particles and inhibited excessive accumulation. As shown in Fig. 2b, SiO₂ microspheres exhibited tightly packed two-dimensional monolayers in a stable hexagonal dense stacking structure. Figure 2c and d display SEM images of self-assembled SiO₂ array after deposition of Au film at different magnifications, revealing that Au@SiO₂ array substrates were successfully fabricated. As seen, AuNPs were tightly covered on the ordered SiO₂ array, resulting in a dramatic increase in the roughness of the surface of SiO₂ microspheres. The Raman spectra of 4-MBA (10⁻⁶ M) labeled Au@SiO₂ array substrate and pure 4-MBA (10⁻¹ M) are shown in Fig. 2e. It was clear to find that 4-MBA (10⁻⁶ M) labeled Au@SiO₂ array substrate exhibited a superior SERS enhancement due to the “hot spots” created by nanogaps between AuNPs on the surface of SiO₂ microspheres. On the contrary, the intensity of pure 4-MBA was very weak. As a characteristic peak of 4-MBA, the intensity at 1594 cm⁻¹ in Fig. 2e was chosen for calculating the enhancement factor (EF) of the Au@SiO₂ array substrate to further scrutinize the SERS activity of the substrate. The formula was as follows: $EF = (I_{SERS}/C_{SERS}) / (I_{RS}/C_{RS})$. Here, $EF = 8.21 \times 10^6$ when $C_{SERS} = 10^{-6}$ M and $C_{RS} = 10^{-1}$ M, showing the substrate owned outstanding SERS enhancement.

The foregoing characterization and analysis showed that the substrate had an ordered array framework and great SERS activity. The uniformity and stability of the substrate were also crucial factors in SERS detection findings. Au@SiO₂ array substrate was ordered and tightly aligned, while voids and stacks still could be rarely seen (Fig. 2c), whose presence might have an impact on the uniformity of the substrate. 4-MBA (10⁻⁴ M) was selected as a Raman reporter with its characteristic peak at 1594 cm⁻¹ for further investigation. The SERS mapping of the substrate was performed with a scan range of 20 × 20 mm² and displayed in the top left corner of Fig. 2f. The color distribution of the SERS mapping was mostly uniform, despite the presence of few blue and yellow, verifying the Au@SiO₂ array substrate was exceedingly homogenous. Furthermore, twenty detection

locations were chosen at random from the Au@SiO₂ array substrate; the obtained spectra are shown in Fig. 2f and the corresponding Raman intensities at 1594 cm⁻¹ are displayed as a bar in Fig. 2g. The relative standard deviation (RSD) was computed as 9.47%, demonstrating that the rare presence of voids and stacks in the structure had no impact on general homogeneity. Finally, 4-MBA labeled Au@SiO₂ array substrate stored at room temperature was tested every 5 days, the outcomes displayed in Fig. 2h. There was no substantial signal degradation seen in the spectra. Figure 2i further illustrates the SERS intensity at 1594 cm⁻¹ decreased by 13.2% after 15 days, confirming the stability of the Au@SiO₂ array substrate. Therefore, the constructed substrate could be employed as a dependable platform for SERS tests.

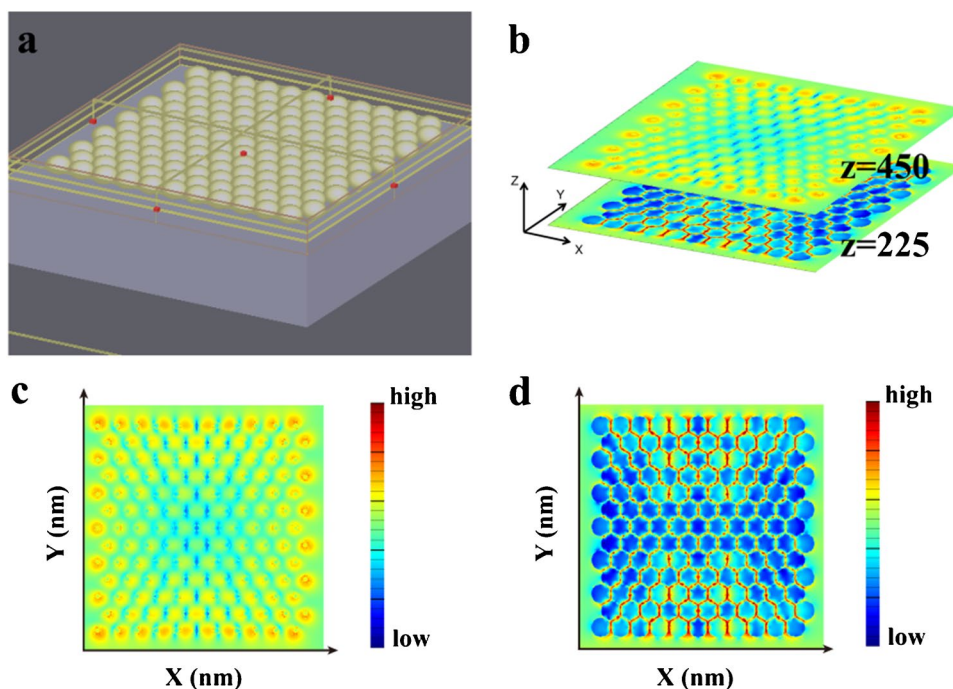
Finite-difference time-domain (FDTD) simulation

The FDTD solution (Lumerical, Inc.) was used to analyze the near-field and far-field electromagnetic response of metals by solving Maxwell's curve equations on a discrete grid. To confirm the spatial electric field distribution of the Au@SiO₂ array substrate after being exposed to a linearly polarized light beam, the FDTD simulation was performed with all geometric parameters adjusted to the average value of the actual sample (Fig. 2c and d). Figure 4a depicts a perspective view of the Au@SiO₂ array substrate model utilized in the simulation. Figure 3b shows a comparison of the typical electric field distribution in the X–Y plane (from top view) on different positions of the Z axis, $z = 450$ nm for the top of Au@SiO₂ array substrate and $Z = 225$ nm for the adjacent; it was evident that the electric field at the top surface of the array had been enhanced (Fig. 3c), but the region with the highest electric field enhancement was located in the gaps between the adjacent SiO₂ microspheres (Fig. 3d). This was because of the fact that the distance between AuNPs on the surface of SiO₂ reduced from the top of the SiO₂ microsphere until the gaps between adjacent SiO₂ microspheres, leading to a gradual increase of LSPR effect. From the two simulation results (Fig. 3b), it could be predicted that the surface of the Au@SiO₂ array substrate was covered by a strong localized electromagnetic field, generating high-density “hot spots.” Thus, the Au@SiO₂ array substrate could exhibit a prominent SERS effect.

FT-IR characterization of SERS tags and capturing substrate

To ensure that SERS tags and capturing substrates were successfully prepared at each step, IR spectroscopy measurements were used. Figure 4a and d are both the FT-IR spectra of AgNCs, and Fig. 4g is the FT-IR spectrum of the Au@SiO₂ array substrate. It was obvious that neither AgNCs nor Au@SiO₂ array substrate, as unmodified

Fig. 3 **a** FDTD simulated the electromagnetic field distribution of Au@SiO₂ array substrate from the perspective view. The electric field distribution collected in the FDTD simulation in different planes. **b** The planes were set in the positions $Z=450$ nm, 225 nm, respectively. The simulated electric field intensity distribution images of the substrate from the upper view when **c** $Z=450$ nm and **d** $Z=225$ nm



nanomaterials, had obvious characteristic peaks. Figure 4b displays the FT-IR spectrum of 4-MBA labeled AgNCs, whereas Fig. 4c is given after the anti-SCCA (labeling) antibodies coupled with 4-MBA labeled AgNCs. When AgNCs were labeled with 4-MBA, only a prominent peak appeared at 1639 cm^{-1} which corresponded to the C=O amide I stretching from the carboxyl group of 4-MBA. The IR peaks at 1251 cm^{-1} , 1557 cm^{-1} , and 1636 cm^{-1} , which were attributed to C-N stretching, N-H amide II stretching, and C=O amide I stretching, respectively, emerged after modification of 4-MBA labeled AgNCs with antibodies. The presence of these peaks indicated that SCCA SERS tags were successfully constructed. Similarly, the FT-IR spectrum revealed a clear peak at 1644 cm^{-1} when AgNCs were tagged with DTNB (Fig. 4e), which matched the C=O stretching vibration of DTNB. The antibodies (anti-CEA (labeling)) were then modified (Fig. 4f), and the vibration peaks of C-N, N-H, and C=O occurred at 1288 cm^{-1} , 1546 cm^{-1} , and 1645 cm^{-1} , proving the antibodies were successfully conjugated with DTNB labeled AgNCs. Figure 4h depicts the FT-IR spectrum of DMSA labeled substrate; the peak at 1646 cm^{-1} corresponded to the C=O amide I stretching of DMSA. There were three peaks in Fig. 4i after being conjugated with antibodies (anti-SCCA (coating) and anti-CEA (coating)), the peak at 1632 cm^{-1} was assigned to C=O, the peak at 1562 cm^{-1} was associated with N-H, and the peak at 1258 cm^{-1} was ascribed to C-N. The existence of these peaks demonstrated the antibodies (coating) had been adhered to the substrate. All in all, the FT-IR

spectra demonstrated that two SERS tags and capturing substrates were all successfully manufactured.

Feasibility of SERS immunoassay on the microfluidic chip

The stability of the prepared SERS tags was verified before the feasibility analysis; a reliable aggregation test was performed. 1 M per liter of NaCl solution was added to the SCCA SERS tag solution and AgNC solution, respectively, for comparative study. The resulting UV-vis absorption spectra are shown in Fig. S3. It could be found that the addition of the salt solution had an effect on the AgNC solution, while there was no significant influence on the SERS tag solution, revealing the stability of SERS tags.

Immediately after the stability of SERS tags was confirmed, two positions of a unit were chosen for SERS measurements to validate the immunoassay process on the microfluidic chip, as shown in Fig. 5a. After adding SERS tags and the serum containing SCCA and CEA into the chip, Fig. 5b is produced. The position I was the inlet of serum where the immunoreaction had not yet started, thus only the peaks of PDMS (685 cm^{-1} , 1413 cm^{-1}) were slightly visible. The serum and SERS tags flowed automatically to the detection chamber (position II), where immunoreaction took place that anti-SCCA (coating) on capturing substrate caught the SCCA which had connected with AgNCs^{4-MBA}@anti-SCCA and anti-CEA (coating) captured the CEA which had linked to AgNCs^{DTNB}@anti-CEA. Accordingly, the spectrum of position II obviously appeared with the characteristic peaks of 4-MBA and DTNB, which

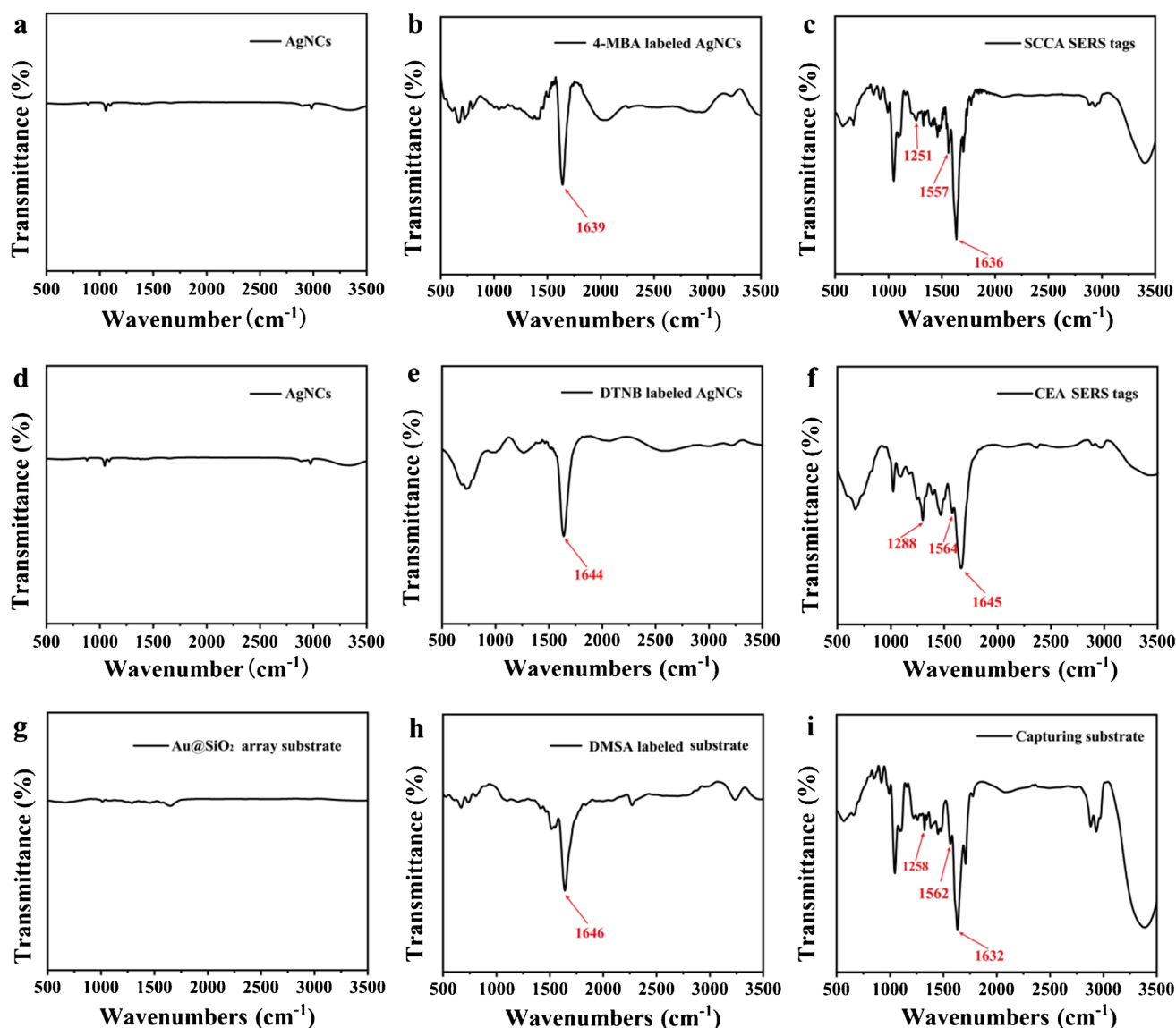


Fig. 4 FT-IR spectra of **a** AgNCs, **b** 4-MBA labeled AgNCs, **c** SCCA SERS tags, **d** AgNCs, **e** DTNB labeled AgNCs, **f** CEA SERS tags, **g** the Au@SiO₂ array substrate, **h** DMSA labeled substrate, **i** capturing substrate

indicated that a large number of SERS tags were trapped on the substrate and the immunocomplexes were formed. Moreover, the signal produced by PDMS could be negligible when compared to those of immunocomplexes. In addition, the signals of the two Raman reporters were distinguished and did not show mutual interference. Consequently, the practicality of the SERS immunoassay was affirmed, and the chip could be applied for the simultaneous detection of SCCA and CEA.

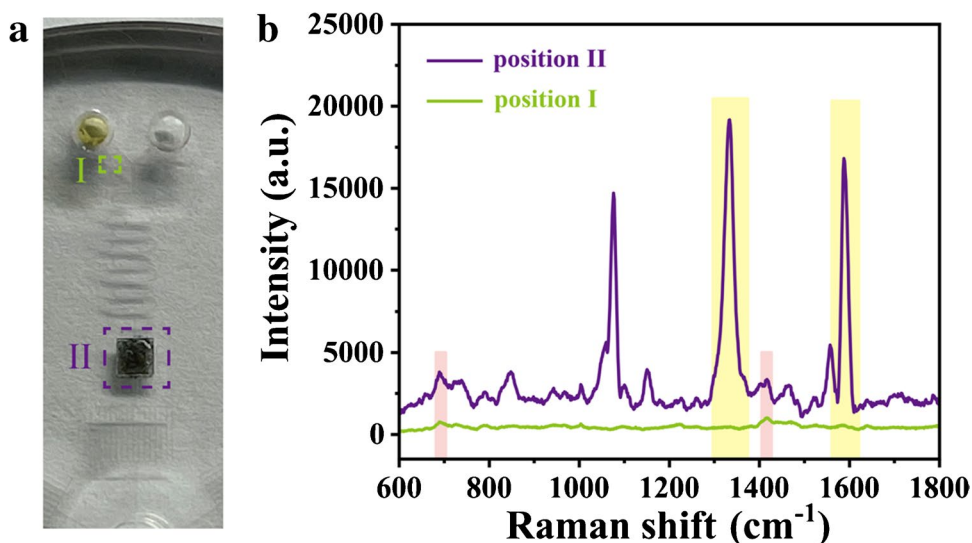
Selectivity and reproducibility of the SERS-based microfluidic chip

The hydrophilicity of the microfluidic chip was firstly tested using red and blue inks with the results shown in Fig. S4.

The inks filled the channel within 30 s, suggesting good hydrophilic treatment. Meanwhile, no leakage was discovered during the test, signifying excellent closure. This test demonstrated the proposed chip could provide autonomous liquid flow without external pumps.

Selectivity is an essential feature of SERS immunoassay studies, as the high selectivity of the assay reduces the likelihood of false positives. In SERS immunoassay, the antigen–antibody reaction was specific, a particular SERS tag would only bind to a specific antigen. In this work, control experiments were carried out with samples containing the same concentration (100 ng mL⁻¹) of different biomarkers (in PBS) to assess the selectivity. The blank sample was pure PBS. Figure 6a depicts the results that samples containing

Fig. 5 **a** Picture of two SERS detection positions on the chip. **b** The corresponding SERS spectra of positions I and II



SCCA exhibited a significant peak at 1594 cm⁻¹, whereas samples containing CEA presented a prominent peak at 1330 cm⁻¹, and no significant SERS signal was observed in other samples. This was because other biomarkers could not be caught by SERS tags and capturing substrate. Figure 6b and c are histograms of the corresponding SERS intensities at 1594 cm⁻¹ and 1330 cm⁻¹, which illustrated that the SERS intensity at 1594 cm⁻¹ was much higher in samples containing SCCA and the SERS intensity at 1330 cm⁻¹ was much higher in samples containing CEA, reflecting only SCCA

and CEA could be captured to form “sandwich” structures on the chip. Furthermore, the faint SERS intensities of samples containing OPN or AFP came from background signals when compared with blank samples. As a consequence, the selectivity of the proposed chip was verified.

The other important aspect of SERS immunoassay research is the reproducibility of the chip. In many circumstances, poor homogeneity of the substrate or the lack of electromagnetic “hot spots” can lead to significant deviation in SERS signal intensity. The reliability and practicability

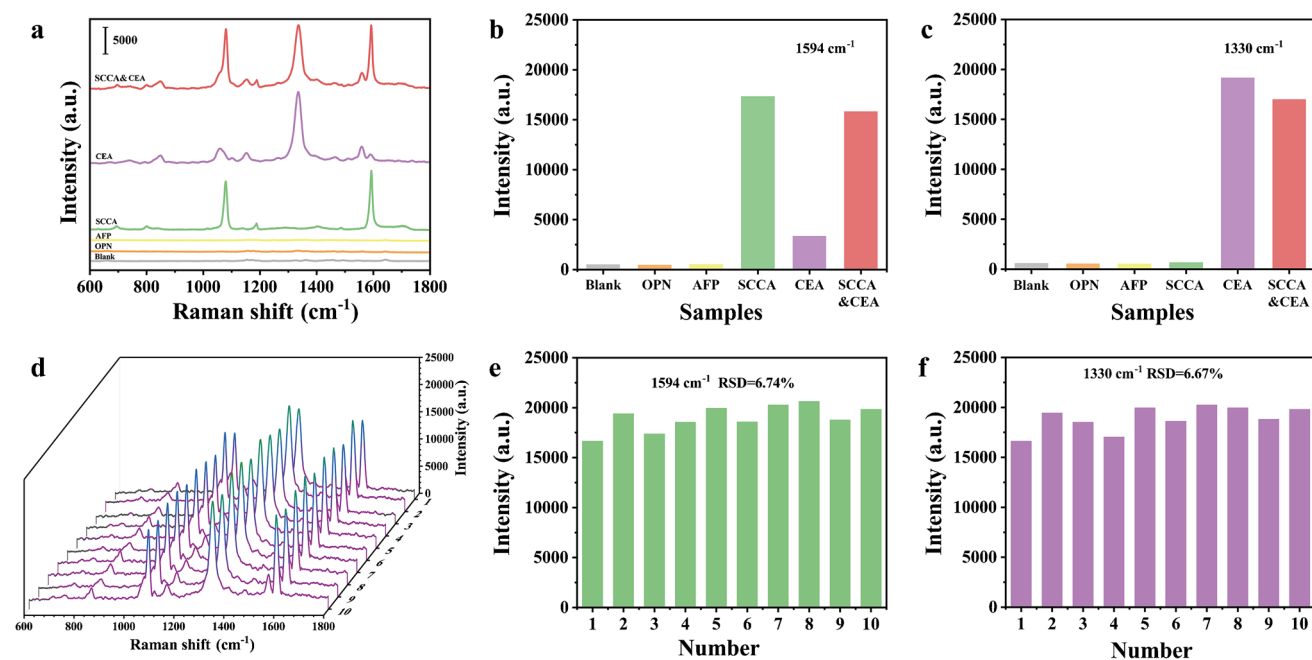


Fig. 6 **a** SERS spectra of blank sample and different protein samples. Histogram of the corresponding SERS intensities at **b** 1594 cm⁻¹ and **c** 1330 cm⁻¹. **d** The SERS spectra of detection on 10 different units.

Histogram of the corresponding SERS intensities at **e** 1594 cm⁻¹ and **f** 1330 cm⁻¹

of the SERS detection are thus significantly impacted by the reproducibility of the chip. Five independent batches of microfluidic chips were manufactured under identical experimental settings, and two units on each chip were randomly selected for detection to test the reproducibility of the chip. Following, ten units were tested using the same samples containing SCCA and CEA, as shown in Fig. 6d. It was evident that the spectral lines produced from the different units essentially overlapped; the locations of the bands were almost equal. The standard variation of the intensities for the peaks at 1594 cm^{-1} and 1330 cm^{-1} , seen in Fig. 6e and f, was lower than 10%, which validated the reproducibility of the chip. Finally, we added additional experiments to verify the reproducibility of the chip in serum. The same went for detecting the same serum samples using ten units of five different batches of SERS-based microfluidic chips. The results are exhibited in Fig. S5. There were no obvious differences in characteristic peak positions and peak intensities (Fig. S5a). To visualize the fluctuations of the SERS signals, Fig. S5b and S5c show the signal intensity histograms for each spectrum at 1594 cm^{-1} and 1330 cm^{-1} . The corresponding relative standard deviations (RSD) were 5.58% and 5.42%, respectively, indicating that the working system in serum was also satisfactorily reproducible. In sum, the developed SERS-based microfluidic chip reflected outstanding properties for practical applications.

Quantitative analysis of SCCA and CEA in PBS and human serum

Different concentrations (from 1 pg mL^{-1} to $1\text{ }\mu\text{g mL}^{-1}$) of SCCA and CEA in PBS and serum were prepared for SERS immunoassay, followed by quantitative analysis using the chip. The SCCA and CEA were dissolved in PBS or blank human serum, respectively, and then continuously diluted to obtain samples with a concentration gradient from 1 pg mL^{-1} to 1 mg mL^{-1} . Figure 7a and d imply that the intensities of SERS signals increased in parallel with the rise in SCCA and CEA concentrations, either in PBS or in serum. Then, the SERS spectra were further investigated by plotting the SERS intensities of characteristic peaks at 1594 cm^{-1} and 1330 cm^{-1} . In Fig. 7b and c, a good linear relationship between the SERS intensities (1594 cm^{-1} and 1330 cm^{-1}) and the logarithm of biomarker concentration (SCCA and CEA in PBS) was observed. The corresponding linear regression equation for SCCA was $y=3033.48x+39,539.97$, with a correlation coefficient of $R^2=0.988$, and for CEA was $y=3224.34x+41,887.87$, with a correlation coefficient of $R^2=0.989$. Similarly, Fig. 7e shows the linear regression equation between SERS intensity at 1594 cm^{-1} and the logarithm of SCCA concentration in serum was $y=2636.53x+34,490.42$, $R^2=0.981$. Figure 7f displays the linear regression equation between SERS intensity

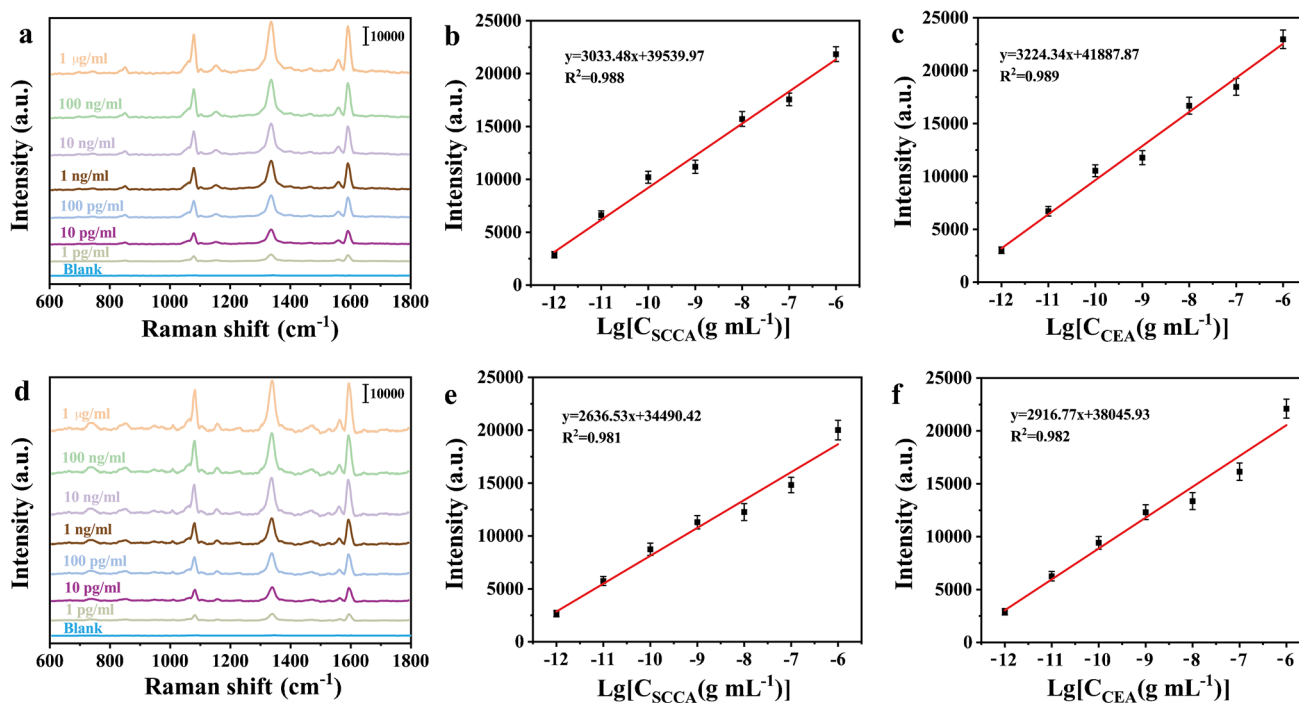


Fig. 7 a Concentration-dependent SERS spectra for SCCA and CEA ($1\text{ }\mu\text{g mL}^{-1}$ to 1 mg mL^{-1} , in PBS). The calibration curves of SERS intensities at 1594 cm^{-1} and 1330 cm^{-1} for the logarithm of the concentration of b SCCA and c CEA in PBS. d Concentration-depend-

ent SERS spectra for SCCA and CEA (1 pg mL^{-1} to $1\text{ }\mu\text{g mL}^{-1}$, in serum). The calibration curves of SERS intensities at 1594 cm^{-1} and 1330 cm^{-1} for the logarithm of the concentration of e SCCA and f CEA in serum

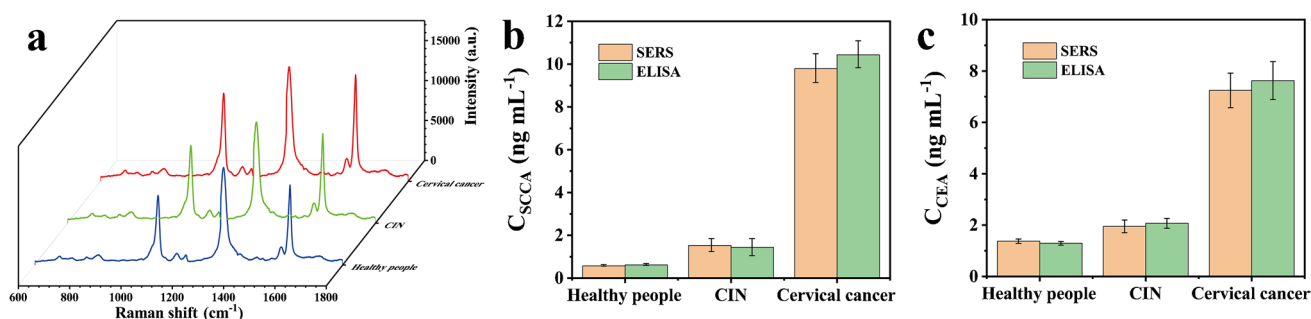


Fig. 8 a The average spectra of each group. The concentration of **b** SCCA and **c** CEA detected by SERS and ELISA

at 1330 cm⁻¹ and the logarithm of CEA concentration in serum was $y = 2916.22x + 38,045.93$, $R^2 = 0.982$. The limits of detection (LODs) for SCCA and CEA in PBS were determined to be 0.37 pg mL⁻¹ and 0.28 pg mL⁻¹, respectively, whereas in human serum were calculated to be 0.45 pg mL⁻¹ and 0.36 pg mL⁻¹, respectively. The LODs were significantly lower than the clinical indexes, 1.5 ng mL⁻¹ for SCCA and 5 ng mL⁻¹ for CEA. A table about the comparison of this work with those previously reported is shown in supporting materials (Table S1). It clearly demonstrated that LODs in our work were much lower than most reported methods, indicating that the proposed chip was more sensitive. Thus, the SERS-based microfluidic chip in this work had an excellent application prospect for the early diagnosis of cancer due to its extremely high sensitivity.

Clinical application

To further validate the potential diagnostic value of the developed SERS-based microfluidic chip, the chip and ELISA were applied to clinical serum samples. A total of 90 serum samples were tested, with 30 each from healthy subjects, CIN patients, and cervical cancer patients. For quantitatively analyzing SCCA and CEA in these practical subjects, the SERS signals of 4-MBA and DTNB were measured, respectively. Figure 8a shows the average SERS spectra for each group of serum samples. It was clearly evident that the SERS signals for both Raman reporters rose with the progression of the disease. Then, the measured SERS intensities at 1594 cm⁻¹ and 1330 cm⁻¹ were fitted to the corresponding regression equation for calculating the SCCA and CEA concentrations. Meanwhile, these clinical serum

samples were assayed by ELISA. The average concentrations of SCCA and CEA for each group were calculated, as listed in Table 2. All RSDs in Table 2 were less than 10%, which showed that the results from the suggested chip were virtually synonymous with the ELISA results. Figure 8b and c show more visually that the results of the SERS microfluidic chip did not differ significantly from those of ELISA kits. In addition, Bland–Altman consistency analysis was used to confirm the fitness of the results provided by the two methods. The results are displayed in Fig. S6, where > 95% of the points fell within the mean \pm 1.96 SD of the difference, indicating that the two methods were in agreement. Hence, the developed chip was potentially employed for early cervical cancer screening by simultaneous detection of SCCA and CEA in serum.

Conclusion

In summary, a novel SERS-based microfluidic chip for simultaneous detection of dual cervical cancer-related biomarkers in real samples was developed. The main innovations of the device were as follows: the design of the Au@SiO₂ array substrate that was placed in the detection chamber of the chip for SERS enhancement, the use of the capillary pump and the hydrophilic treatment of channels for pump-free flow, and the multi-channel design for parallel detection. When using the suggested SERS-based microfluidic chip for assay, the LODs of SCCA and CEA in PBS were as low as 0.37 pg mL⁻¹ and 0.28 pg mL⁻¹, and in human serum reached 0.45 pg mL⁻¹ and 0.36 pg mL⁻¹, respectively. Furthermore, the chip was effectively utilized for detecting

Table 2 The results of SERS and ELISA for clinical samples

Sample	SERS (ng mL ⁻¹)		ELISA (ng mL ⁻¹)		Relative error (%)	
	SCCA	CEA	SCCA	CEA	SCCA	CEA
Healthy people	0.572	1.376	0.615	1.293	-6.992	6.419
CIN	1.525	1.951	1.439	2.068	5.976	-5.658
Cervical cancer	9.786	7.247	10.435	7.625	-6.621	-4.957

clinical samples, with results that were comparable to commercial ELISA kits. The proposed biosensor demonstrated high sensitivity and accuracy in this work, making it a promising device for cervical cancer diagnosis.

Supplementary Information The online version contains supplementary material available at <https://doi.org/10.1007/s00216-022-04296-w>.

Funding This work was supported by the National Natural Science Foundation of China (No. 82072088), the Social Development Foundation of Jiangsu (No. BE2018684), Yangzhou Science and Technology Project (No. YZ2017075), Contract for Maternal and Child Health Research Projects in Jiangsu Province (No. F201809), Postgraduate Research & Practice Innovation Program of Jiangsu Province (No. SJCX22_1820), High-end talent support program of Yangzhou University, and the QingLan Project of Yangzhou University.

Declarations

Ethical approval This work followed the ethical principles of medical research in the Helsinki declaration. All serum samples were collected with the approval of the Ethics Committee of Yangzhou University School of Clinical Medicine, China. And all donors signed an informed consent before serum collection.

Conflict of interest The authors declare no competing interests.

References

- Small W Jr, Bacon MA, Bajaj A, Chuang LT, Fisher BJ, Harkenrider MM, et al. Cervical cancer: a global health crisis. *Cancer*. 2017;123(13):2404–12.
- Castle PE, Einstein MH, Sahasrabudhe VV. Cervical cancer prevention and control in women living with human immunodeficiency virus. *Cervical cancer prevention and control in women living with human immunodeficiency virus*. CA-Cancer J Clin. 2021;71(6):505–26.
- Cohen PA, Jhingran A, Oaknin A, Denny L. Cervical cancer. *Lancet*. 2019;393(10167):169–82.
- Pfaendler KS, Tewari KS. Changing paradigms in the systemic treatment of advanced cervical cancer. *Am J Obstet Gynecol*. 2016;214(1):22–30.
- Zhu H. Squamous cell carcinoma antigen: clinical application and research status. *Diagnostics*. 2022;12(5):1065.
- Colombo N, Carinelli S, Colombo A, Marini C, Rollo D, Sessa C. Cervical cancer: ESMO Clinical Practice Guidelines for diagnosis, treatment and follow-up. *Ann Oncol*. 2012;23:27–32.
- Hao C, Zhang GQ, Zhang LJ. Serum CEA levels in 49 different types of cancer and noncancer diseases. In: Zhang L, editor. *Glycans and glycosaminoglycans as clinical biomarkers and therapeutics*, PT A. 2019;162:213–27.
- Tendler A, Kaufman HL, Kadish AS. Increased carcinoembryonic antigen expression in cervical intraepithelial neoplasia grade 3 and in cervical squamous cell carcinoma. *Hum Pathol*. 2000;31(11):1357–62.
- Huang G, Chen R, Lu N, Chen Q, Lv W, Li B. Combined evaluation of preoperative serum CEA and CA125 as an independent prognostic biomarker in patients with early-stage cervical adenocarcinoma. *Oncotargets Ther*. 2020;13:5155–64.
- Akama K, Iwanaga N, Yamawaki K, Okuda M, Jain K, Ueno H, et al. Wash- and amplification-free digital immunoassay based on single-particle motion analysis. *ACS Nano*. 2019;13(11):13116–26.
- Ragone A, Salzillo A, Spina A, Zappavigna S, Caraglia M, Sapio L, et al. Protein kinase a detection in human urine samples. *J Clin Med*. 2021;10(18):4096.
- Sethi MK, Hancock WS, Fanayan S. Identifying N-glycan biomarkers in colorectal cancer by mass spectrometry. *Acc Chem Res*. 2016;49(10):2099–106.
- Wang ZL, Wang ZY, Zong SF, Cui YP. Microfluidic SERS chip and its biosensing applications. *Chinese Optics*. 2018;11(3):513–30.
- Huang JA, Zhang YL, Ding H, Sun HB. SERS-enabled lab-on-a-chip systems. *Adv Opt Mater*. 2015;3(5):618–33.
- Wang CY, Mu XQ, Huo J, Zhang B, Zhang KY. Highly-efficient SERS detection for *E. coli* using a microfluidic chip with integrated NaYF₄:Yb, Er@SiO₂@Au under near-infrared laser excitation. *Microsyst Technol*. 2021;27(9):3285–91.
- Oliveira MJ, Cunha I, de Almeida MP, Calmeiro T, Fortunato E, Martins R, et al. Reusable and highly sensitive SERS immunoassay utilizing gold nanostars and a cellulose hydrogel-based platform. *J Mater Chem B*. 2021;9(36):7516–29.
- Zhou W, Tian YF, Yin BC, Ye BC. Simultaneous surface-enhanced Raman spectroscopy detection of multiplexed micro-RNA biomarkers. *Anal Chem*. 2017;89(11):6121–9.
- Hung LY, Wu HW, Hsieh K, Lee GB. Microfluidic platforms for discovery and detection of molecular biomarkers. *Microfluid Nanofluid*. 2014;16(5):941–63.
- Mishra R, Zapatero-Rodríguez J, Sharma S, Kelly D, McAuley D, Gilgunn S, et al. Automation of multi-analyte prostate cancer biomarker immunoassay panel from whole blood by minimum-instrumentation rotational flow control. *Sensor Actuat B-Chem*. 2018;263:668–75.
- Ahi EE, Torul H, Zengin A, Sucularlı F, Yıldırım E, Selbes Y, et al. A capillary driven microfluidic chip for SERS based hCG detection. *Biosens Bioelectron*. 2022;195: 113660.
- Gao R, Lv Z, Mao Y, Yu L, Bi X, Xu S, et al. SERS-based pump-free microfluidic chip for highly sensitive immunoassay of prostate-specific antigen biomarkers. *ACS Sensors*. 2019;4(4):938–43.
- Chen PC, Cheng YF, Young KC, Hsieh HL, Yang CL. Design and characterization of a capillary-driven and parallelized microfluidic chip for distributing a liquid plug. *Int J Precis Eng Manuf*. 2016;17(11):1547–54.
- Guo J, Zeng F, Guo J, Ma X. Preparation and application of microfluidic SERS substrate: challenges and future perspectives. *J Mater Sci Technol*. 2020;37:96–103.
- Wang CY, Xu Y, Wang R, Zhao HZ, Xiang ST, Chen L, et al. Fabrication and effect study of microfluidic SERS chip with integrated surface liquid core optical waveguide modified with nano gold. *Microsyst Technol*. 2017;23(8):3059–68.
- Wang L, Zhou G, Xi Guan, Zhao L. Rapid preparation of surface-enhanced Raman substrate in microfluidic channel for trace detection of amoxicillin. *Spectrochim Acta A*. 2020;235:118262.
- Zhu C, Meng G, Zheng P, Huang Q, Li Z, Hu X, et al. A hierarchically ordered array of silver-nanorod bundles for surface-enhanced Raman scattering detection of phenolic pollutants. *Adv Mater*. 2016;28(24):4871–6.
- Xu S, Li H, Guo M, Wang L, Li X, Xue Q. Liquid-liquid interfacial self-assembled triangular Ag nanoplate-based high-density and ordered SERS-active arrays for the sensitive detection of dibutyl phthalate (DBP) in edible oils. *Analyst*. 2021;146(15):4858–64.
- Fu H, Bao H, Zhang H, Zhao Q, Zhou L, Zhu S, et al. Quantitative surface-enhanced Raman spectroscopy for field detections based on structurally homogeneous silver-coated silicon nanocone arrays. *ACS Omega*. 2021;6(29):18928–38.
- Fu Q, Liu HL, Wu Z, Liu A, Yao C, Li X, et al. Rough surface Au@Ag core-shell nanoparticles to fabricating high sensitivity

- SERS immunochromatographic sensors. *J Nanobiotechnol.* 2015;13(1):81.
30. Chen YK, Li H, Chen JM, Li D, Zhang MY, Yu GH, et al. Self-generating nanogaps for highly effective surface-enhanced Raman spectroscopy. *Nano Res.* 2022;15(4):3496–503.
 31. Choi H-K, Park S-M, Jeong J, Lee H, Yeon GJ, Kim D-S, et al. Spatially controlled fabrication of surface-enhanced Raman scattering hot spots through photoinduced dewetting of silver thin films. *J Phys Chem Lett.* 2022;13(13):2969–75.
 32. Perassi EM, Coronado EA. The structure, energy, confinement, and enhancement of hot spots between two nanoparticles. *J Phys Chem C.* 2013;117(15):7744–50.
 33. Pu H, Huang Z, Xu F, Sun DW. Two-dimensional self-assembled Au-Ag core-shell nanorods nanoarray for sensitive detection of thiram in apple using surface-enhanced Raman spectroscopy. *Food Chem.* 2021;343: 128548.
 34. Chang YH, Hsu WH, Wu SL, Ding YC. The synthesis of a gold nanodisk-molecular layer-gold film vertical structure: a molecular layer as the spacer for SERS hot spot investigations. *Mater Chem Front.* 2017;1(5):922–7.
 35. Hu Y, Wang X, Zhang M, Wang S, Li S, Chen G. A hierarchical anodic aluminum oxide template. *Nano Lett.* 2021;21(1):250–7.
 36. Zhang QA, Li WY, Moran C, Zeng J, Chen JY, Wen LP, et al. Seed-mediated synthesis of Ag nanocubes with controllable edge lengths in the range of 30–200 nm and comparison of their optical properties. *J AM Chem Soc.* 2010;132(32):11372–8.
 37. Stöber W, Fink A, Bohn E. Controlled growth of monodisperse silica spheres in the micron size range. *J Colloid Interf Sci.* 1968;26(1):62–9.
 38. Kondo M, Shinozaki K, Bergstroem L, et al. Preparation of colloidal monolayers of alkoxyated silica particles at the air-liquid interface. *Langmuir.* 1955;11:394–7.
 39. Kagawa R, Takeyasu N, Kaneta T, Takemoto Y. Oil-in-water emulsion as fabrication platform for uniform plasmon-controlled two-dimensional metallic nanoparticle array. *Appl Phys Express.* 2016;9(7):075003.
- Publisher's note** Springer Nature remains neutral with regard to jurisdictional claims in published maps and institutional affiliations.
- Springer Nature or its licensor holds exclusive rights to this article under a publishing agreement with the author(s) or other rightsholder(s); author self-archiving of the accepted manuscript version of this article is solely governed by the terms of such publishing agreement and applicable law.